JOURNAL OF SPACECRAFT AND ROCKETS
Vol. 40, No. 6, November–December 2003

Engineering Notes

ENGINEERING NOTES are short manuscripts describing new developments or important results of a preliminary nature. These Notes cannot exceed six manuscript pages and three figures; a page of text may be substituted for a figure and vice versa. After informal review by the editors, they may be published within a few months of the date of receipt. Style requirements are the same as for regular contributions (see inside back cover).

Station Collocation Design Algorithm for Multiple Geostationary Satellites Operation

Bong-Kyu Park,* Min-Jea Tahk,† and Hyo-Choong Bang‡
Korea Advanced Institute of Science and Technology, Daejon 305-701, Republic of Korea
and
Sung-Bong Choi§
Korea Aerospace Research Institute, Daejon 305-333, Republic of Korea

Introduction

A STATION collocation technique has been employed to avoid the possibility of collision or radiometric interference for the operation of multiple geostationary satellites located at the neighboring longitude slots. Applications of the station collocation strategy for two satellites are widely known and have been implemented successfully. Nevertheless, the increasing number of operating geostationary satellites allows us only the limited geostationary orbital space, which in turn urges multiple satellite collocation strategies controlling more than three satellites simultaneously.

Research on the multiple satellite collocation has been presented through many papers, but their analyses were largely focused on case-by-case studies by assuming a fixed number of control satellites.[1–5] This Note proposes a useful station collocation design algorithm for station collocation of an arbitrary number of satellites. Change in the satellite numbers does not essentially affect the structure of the proposed algorithm. The new technique optimally allocates eccentricity control circle positions for each satellite by adopting a virtual dynamic model approach.

Conventional Collocation Strategy for Two Satellites

Orbit normal separation distance between two neighboring satellites can be maintained by targeting inclination vectors of each satellite to different directions. Also the radial separation is accomplished by targeting each eccentricity vector to different directions. But, if the radial and normal separation methods are applied separately there always exist two points where the separation distance becomes zero. Therefore, generally station collocation methods maintain the separation distance by properly combining the radial and orbit normal separation strategy.

Because of the small eccentricity and inclination of tgeostationary satellites, the eccentricity and inclination vectors can be expressed as $\boldsymbol{e} = [e_x, e_y]^T$ and $\boldsymbol{i} = [i_x, i_y]^T$ in the Earth-centered inertial (ECI) coordinate in which the x axis points the vernal equinox, the z axis is parallel to the Earth spin axis, and the y axis is selected to from the right-hand coordinate system. They are defined by

$$e_y = e\sin(\Omega + \omega), \qquad e_x = e\cos(\Omega + \omega) \tag{1}$$

$$i_x = i\cos\Omega, \qquad i_y = i\sin\Omega \tag{2}$$

where e is the eccentricity, Ω denotes the right ascension of ascending node, ω is the argument of perigee, and i is the inclination of the orbit with respect to the equatorial plane. The relative minimum distance between two satellites, projected onto the meridian plane, was derived by Eckstein[6] and can be summarized as follows. The meridian plane is defined as a plane that intersects the north pole, the south pole, and the targeted stationkeeping box center. The relative distance between any two adjacent satellites, projected onto the meridian plane, is

$$D = [\Delta r^2 + \Delta n^2]^{\frac{1}{2}} \tag{3}$$

where Δr is the radial distance and Δn is the out-of-plane distance; Δr and Δn are described as follows:

$$\Delta r = r_1 - r_2 \approx a_s/(1 + e_1\cos M_1) - a_s/(1 + e_2\cos M_2) \approx a_s(e_1\cos M_1 - e_2\cos M_2) \tag{4}$$

$$\Delta n = n_1 - n_2 \approx a_s\sin(\omega_1 + M_1)i_1 - a_s\sin(\omega_2 + M_2)i_2 \tag{5}$$

where a_s is the unperturbed geostationary semimajor axis similar to distance from the Earth center, ω is argument of perigee, and M denotes the mean anomaly. After some algebraic manipulation considering the geometric relations

$$\gamma = \Omega + \omega + M \tag{6}$$

$$\cos M = e_x\cos\gamma + e_y\sin\gamma \tag{7}$$

$$\cos(\omega + M) = i_x\sin\gamma - i_y\cos\gamma \tag{8}$$

where γ is the right ascension of the stationkeeping box center and Ω is the right ascension of the ascending node, the radial and out-of-plane components could be expressed as

$$\Delta r = a_s(-\Delta e_x\cos\gamma - \Delta e_y\sin\gamma) \tag{9}$$

$$\Delta n = a_s(\Delta i_x\sin\gamma - \Delta i_y\cos\gamma) \tag{10}$$

where the symbol Δ denotes element differences between two satellites. Substitution of Eqs. (9) and (10) into Eq. (3) yields

$$D^2 = \left(\tfrac{1}{2}\right)a_s^2\left[\Delta i_x^2 + \Delta i_y^2 + \Delta e_y^2 + \left(\Delta e_x^2 - \Delta e_y^2 - \Delta i_x^2 + \Delta i_y^2\right)\cos 2\gamma + 2(\Delta e_x\Delta e_y - \Delta i_x\Delta i_y)\sin 2\gamma\right] \tag{11}$$

Received 11 May 2003; revision received 31 July 2003; accepted for publication 26 August 2003.

*Senior Researcher, Communication Satellite Systems Department; currently Research Engineer, Korea Aerospace Research Institute, 45 Eoeun-Dong, Youseong-Gu, Daejon 305-333, Republic of Korea.

†Professor, Flight Dynamic and Control Laboratory, Department of Aerospace Engineering, 373-1 Kusong Yuseong-Gu. Member AIAA.

‡Associate Professor, Flight Dynamic and Control Laboratory, Department of Aerospace Engineering, 373-1 Kusong Yuseong-Gu. Member AIAA.

§Director, Communication, Ocean and Meteorological Program Office, 45 Eoeun-Dong, Youseong-Gu.

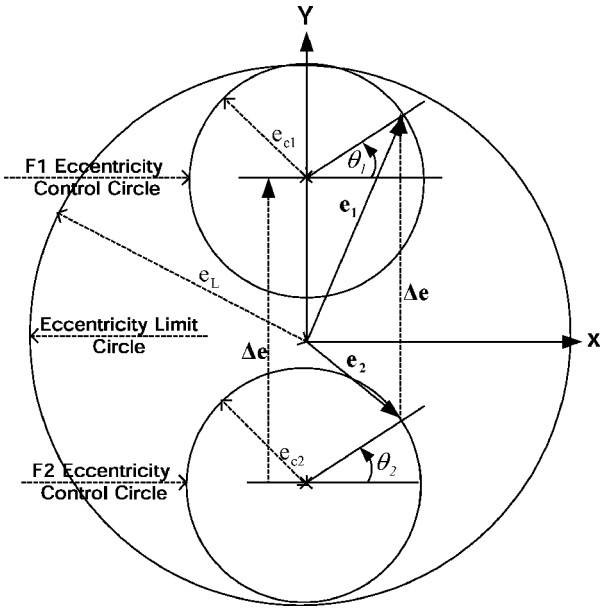

Fig. 1 Radial separation method using eccentricity control.

The minimum distance between two satellites $D_{\min}$ could be derived by taking partial differentiation of D with respect to γ, and the result is

$$D_{\min} = \frac{\sqrt{2}a_s|\Delta e \Delta i \cos\theta|}{\left[\Delta e^2 + \Delta i^2 + (\Delta e^4 + \Delta i^4 - 2\Delta e^2 \Delta i^2 \cos 2\theta)^{\frac{1}{2}}\right]^{\frac{1}{2}}} \tag{12}$$

where θ is the offset angle between the eccentricity vector difference and the inclination vector difference. For given Δi and Δe, θ maximizing $D_{\min}$ is obtained from

$$\frac{\partial D_{\min}}{\partial \theta} = 0 \tag{13}$$

and the result turns out to be the solution $\theta = 0$ or 180 deg. It is evident from Eq. (12) that if $\theta = 90$ deg, the minimum distance becomes zero. Namely, to ensure the separation distance between the two satellites the eccentricity vector difference and the inclination vector difference should be aligned parallel:

$$(\boldsymbol{e}_1 - \boldsymbol{e}_2) \cdot (\boldsymbol{i}_1 - \boldsymbol{i}_2) = \pm|\boldsymbol{e}_1 - \boldsymbol{e}_2||\boldsymbol{i}_1 - \boldsymbol{i}_2| \tag{14}$$

Once the geometric relations presented in Fig. 1 including eccentricity limit circles and eccentricity control circles are met, this requirement is substantially satisfied.

In Fig. 1 the x and y axes are identical to those of the ECI coordinates. The eccentricity limit circle defines the maximum eccentricity allowed depending on the stationkeeping box allocation strategy for each satellite. If the physical dimensions of each satellite are significantly different or the mission policies are different, different size of eccentricity limit circles could be applied for two satellites. The eccentricity control circle defines the area in which the eccentricity vectors are actually controlled to reside, using the east/west stationkeeping maneuvers.

As mentioned before, the eccentricity control circle centers are aligned along the inclination vector difference. In Fig. 1 $\Delta \boldsymbol{e}$ is parallel with the y axis because it is assumed that $\Delta \boldsymbol{i}$ is controlled to point the y axis through the north/south stationkeeping.

The eccentricity control circles are located to contact with limit circle to split the two eccentricity control circles to the longest possible. The eccentricity vector tips are forced to move along the eccentricity circle anticlockwise once a year by periodic east/west stationkeeping maneuvers. The angular positions of two eccentricity vector tips from the eccentricity control circle center are controlled to be identical for two satellites to satisfy the condition in Eq. (14), that is, $\theta_1 = \theta_2$ in Fig. 1. Usually, the angular positions of the eccentricity vector θ_1 and θ_2 are targeted to the right ascension of the sun. The eccentricity circle position and size are the major parameters for station collocation planning.

When the condition of Eq. (14) is satisfied, the minimum distance of Eq. (12) is simplified into

$$D_{\min} = a_s \min(|\Delta e|, |\Delta i|) \tag{15}$$

Usually, the stationkeeping box allocation result produces $|\Delta e|$ less than $|\Delta i|$ so that the minimum distance $D_{\min}$ is simplified to

$$D_{\min} = a_s|\Delta e| \tag{16}$$

From Eq. (16) it can be realized that the minimum distance $D_{\min}$ is only proportional to the eccentricity vector difference when the condition defined by Eq. (14) is satisfied. Thus bigger $|\Delta e|$ guarantees longer separation distance between satellites.

From the geometry of Fig. 1, Δe is related by

$$\Delta e = 2(e_L - e_c) \tag{17}$$

where e_L denotes the eccentricity limit circle radius and e_c indicates the eccentricity control circle radius. Then, e_L is determined in the stationkeeping box allocation stage, and kept unchanged. We can see that better separation distance could be achieved by reducing e_c. However, careful consideration should be given in sizing e_c because of the following reason. The yearly minimum ΔV budget, required for eccentricity control only, is approximated by

$$\Delta V_{\text{year}} \approx \pi V_s |e_{\text{ss}} - e_c| \tag{18}$$

where V_s denotes velocity of the unperturbed geostationary satellite and e_{ss} is the steady-state eccentricity circle.[7] The steady-state eccentricity circle corresponds to a circular type locus of the eccentricity vector tip developed by solar pressure in the absence of corrective force. Note that decreasing the eccentricity control circle size increases the ΔV requirement and the minimum separation distance as Eqs. (16) and (17). Therefore, some tradeoff study should be conducted between the fuel budget and the minimum separation distance for the selection of the eccentricity control circle size.

Collocation Strategy for Multiple Satellites

Station collocation for arbitrary number of satellites is also achievable by locating each eccentricity and inclination vector to satisfy the relationship described in Eq. (14). An additional key technical issue to be considered is to construct a consistent eccentricity control circle position algorithm unaffected by the number of satellites to be collocated as well as satellite parameters. As mentioned before, the position and size of the eccentricity control circle are the major design parameters in the station collocation. In this study it is assumed that the eccentricity control sizes were already determined through a tradeoff study between fuel consumption and minimum separation distance. First let us define $\boldsymbol{d}_{\text{ci}}$ as the eccentricity control circle position vector for the ith satellite. For given inclination vector $\boldsymbol{i}_i$, eccentricity control circle size e_{ci}, and eccentricity limit circle size e_{Li}, the optimal station collocation performance for n satellites, is described as

$$\max_{d_{\text{ci}}} \sum_{i,j=1}^{n} D_{\min ij}(\boldsymbol{d}_{\text{ci}}, \boldsymbol{d}_{\text{cj}}, e_{\text{ci}}, e_{\text{cj}}, e_{\text{Li}}, e_{\text{Lj}}, \boldsymbol{i}_i, \boldsymbol{i}_j) \tag{19}$$

The preceding objective is achieved when the eccentricity control circles satisfy the following three conditions.

Condition 1: The difference vectors between the eccentricity control circle center position vectors should be aligned parallel with the difference vectors of their inclination vectors. This condition can be expressed as

$$(\boldsymbol{e}_i - \boldsymbol{e}_j) \cdot (\boldsymbol{i}_i - \boldsymbol{i}_j) = \pm|\boldsymbol{e}_i - \boldsymbol{e}_j||\boldsymbol{i}_i - \boldsymbol{i}_j| \tag{20}$$

As described earlier, this condition is required to place the maximum radial separation 90 deg away from the normal separation in orbit phase angle.

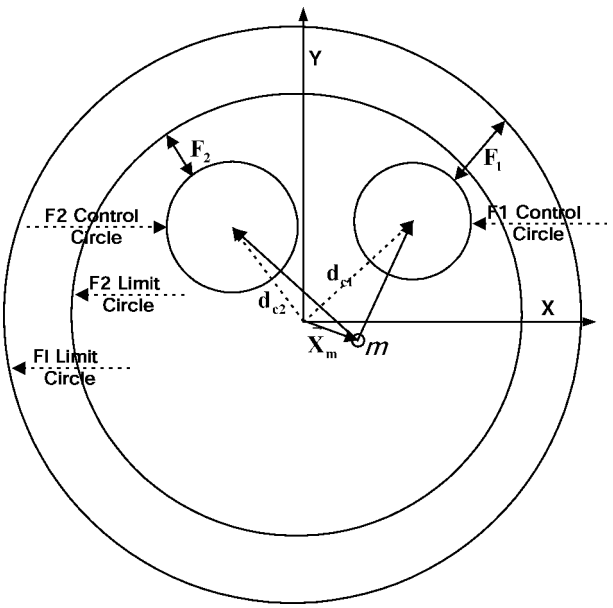

Fig. 2 Virtual dynamic system for optimal eccentricity control circle position determination.

Condition 2: Each eccentricity control circle should reside within the area defined by the eccentricity limit circles. This condition is needed to confine the magnitude of the eccentricity in a predefined range.

Condition 3: The eccentricity control circle positions should be adjusted so that the distances between eccentricity control circles are separated to the maximum length possible. This condition guarantees the maximum separation distance between satellites for given conditions.

There could be many different approaches possible to find a solution satisfying these conditions. An analytical solution might be feasible for a fixed number of satellites as the two-satellite collocation problem described in the beginning. However, the approach cannot be extended into a different number of satellites collocation problems, and a different approach needs to be found with careful consideration.

In this Note selection of the eccentricity control circle positions satisfying those three conditions are realized using a virtually devised dynamic system shown in Fig. 2. Hereafter, the term "virtual dynamics" is used to indicate this virtually devised dynamic system.

The assumed dynamic model consists of the eccentricity control circles, the limit circles, and a virtual point mass. The relative position of the eccentricity circle centers with respect to the virtual point mass, spreads out at a constant rate, and moves to find a best fit to eccentricity limit circles. The movement continues until no more growth is allowed by the constraint given by the eccentricity limit circles. During the adjustment, the relative position between the eccentricity control circles and a point mass are always maintained in the same shape. In Fig. 2 each satellite possesses different sizes of the eccentricity control circle and a limit circle, to consider different operation parameters for each satellite, to consider the situation of applying different operation parameters for each satellite, which might occur more often when the number of the controlling satellite increases.

To meet condition 1, the initial positions of the eccentricity control circle center $\boldsymbol{d}_{\mathrm{ci}}$ are determined by adding the scaled target inclination vector $\alpha \boldsymbol{i}_i$ to the arbitrary base position $\boldsymbol{x}_m$, such as

$$\boldsymbol{d}_{\mathrm{ci}} = \boldsymbol{x}_m + \alpha \boldsymbol{i}_i \tag{21}$$

where α and $\boldsymbol{i}_i$ denote the scale factor and the target inclination vector, respectively. The target inclination vector $\boldsymbol{i}_i$ should be given as an input parameter. The point mass position vector $\boldsymbol{x}_m$ is initialized to be located at the origin of the coordinate system and forced to move by the virtual dynamics described later in detail. Condition 1 is always satisfied by Eq. (21) for an arbitrary α. In other words,

$$\boldsymbol{e}_i - \boldsymbol{e}_j \approx \boldsymbol{d}_{\mathrm{ci}} - \boldsymbol{d}_{\mathrm{cj}} = \alpha(\boldsymbol{i}_i - \boldsymbol{i}_j) \tag{22}$$

Therefore, Eq. (20) is satisfied by $\boldsymbol{d}_{\mathrm{ci}}$ selected by Eq. (21).

Conditions 2 and 3 are satisfied by a judicious selection of α and $\boldsymbol{x}_m$ values. For the selection of α and $\boldsymbol{x}_m$, we adopt a virtual mass m located at $\boldsymbol{x}_m$. The virtual mass is forced to move by the virtual force interacting between the control circle and the limit circle. The virtual dynamics are described as

$$m\ddot{\boldsymbol{x}}_m + c\dot{\boldsymbol{x}}_m = \sum_i \boldsymbol{F}_i \tag{23}$$

where the damping coefficient c contributes to improving the convergence rate by removing the osculating motion. The size of the interaction forces is assumed to be inversely proportional to the minimum distance between the eccentricity control circle and the limit circle cord and vertically active on the control circle cord:

$$\boldsymbol{F}_i = -\left[k/(e_{\mathrm{Li}} - d_{\mathrm{ci}} - e_{\mathrm{ci}})^2\right](\boldsymbol{d}_{\mathrm{ci}}/d_{\mathrm{ci}}) \tag{24}$$

where e_{Li}, d_{ci}, e_{ci} represent the size of the limit circle, the distance of the eccentricity control circle center from the origin, and the size of the eccentricity control circle for the ith satellite. The parameter k represents an arbitrary constant adopted for scaling purpose. The inversely proportional force is assumed to confine the eccentricity control circle within the eccentricity limit circle and to move the point mass to the equilibrium point, which makes best fit to eccentricity limit circles. For example when the eccentricity control circles are positioned on the right side, the inversely proportional force will try to move them to the left side because the distance to the limit circle cord is shorter on the right side than the left side. It is assumed that the moment causing the rotational motion does not exist; in other words, the resultant force $\sum \boldsymbol{F}_i$ acts exactly on point mass m. The rotational motion represents angular motion of the eccentricity control circle position around the virtual point mass. If the rotational motion is allowed, the constraint given by Eq. (20) cannot be satisfied.

For current $\boldsymbol{x}_m$ the maximum α satisfying condition 2 can be derived after simple algebraic calculation:

$$|\boldsymbol{x}_m + \alpha_{\max i}\boldsymbol{i}_i| = e_{\mathrm{Li}} - e_{\mathrm{ci}} \tag{25}$$

$$\alpha_{\max} = \min(\alpha_{\max i}) \tag{26}$$

From the eccentricity control circle and limit circle of each satellite, $\alpha_{\max i}$ is calculated from Eq. (25). The maximum value among $\alpha_{\max i}$ is selected as $\alpha_{\max}$. After selection of $\alpha_{\max}$, α_{k+1} is determined as follows:

$$\alpha_{k+1} = \alpha_k + K(\alpha_{\max} - \alpha_k), \qquad \alpha_0 = 0,\ (0 < K \ll 1) \tag{27}$$

Thus, α_{k+1} corresponds to the eccentricity control circle position from Eq. (21) at the $k+1$ step. The constant K is employed to avoid possible dynamic divergence caused from excessive virtual interaction force.

Once the eccentricity control circle positions are determined, the virtual interaction forces are calculated from Eq. (24). Then numerical integration of the virtual dynamics in Eq. (23) is conducted for the next step. The iteration continues until the following condition is satisfied:

$$\alpha_{k+1}/\alpha_{\max} \geq 0.99999 \tag{28}$$

Figure 3 summarizes the proposed algorithm for the optimal position determination of the eccentricity control circle.

After decision of the eccentricity control circle positions, the eccentricity vectors are targeted to the following value:

$$\boldsymbol{e}_i = \boldsymbol{d}_{\mathrm{ci}} + e_{\mathrm{ci}}\cos\theta_s \boldsymbol{i} + e_{\mathrm{ci}}\sin\theta_s \boldsymbol{j} \tag{29}$$

where θ_s represents the right ascension of the sun growing from 0 to 2π for a year and $\boldsymbol{i}$ and $\boldsymbol{j}$ denote unit vectors pointing x and y axes, respectively. It is easily found that $\boldsymbol{e}_i$ is repeated every year because $\boldsymbol{d}_{\mathrm{ci}}$ is externally fixed after the final decision.

Table 1 Station collocation parameters

Satellite ID	e_{ss}	e_L	e_c
0	2.2282$E-4$	1.9300$E-4$	2.227$E-5$
1	1.9165$E-4$	2.3488$E-4$	2.227$E-5$
2	2.0987$E-4$	1.9300$E-4$	2.227$E-5$

Table 2 Stationkeeping schedule

Day	Satellite 0 mission	Satellite 1 mission	Satellite 2 mission
1	N/S SK	——	——
2	——	N/S SK	——
3	E/W SK	——	N/S SK
4	——	E/W SK	——
5	——	——	E/W SK
10	E/W SK	——	——
11	——	E/W SK	——
12	——	——	E/W SK
15	N/S SK	——	——

Table 3 Target inclination vector

Satellite ID	i_x	i_y
0	0.001	0.001
1	−0.030	0.015
2	−0.030	−0.015

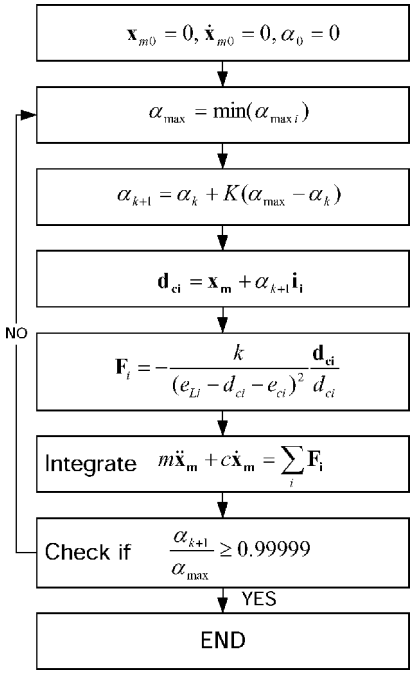

Fig. 3 Optimal eccentricity control circle position selection algorithm.

Simulation Results

For verification of the proposed technique, the new algorithm is applied to a three-satellite collocation problem. As mentioned before, the proposed algorithm is applicable to an arbitrary number of satellites collocation problem by simple modification of the satellite index number n. However, in this example our analysis is limited to only a three-satellites collocation problem on account of limited space. Table 1 summarizes the parameters selected for the simulation study. The parameters for satellite 0 and satellite 1 are selected from two actual geostationary satellites data. The stationkeeping schedule is also established by extending that of the two satellites, and the result is summarized in Table 2. The target inclination vectors for three satellites are selected in a triangular shape as presented in Table 3. Figure 4 shows the position of the eccentricity control circles calculate by the new approach. It is not difficult to notice that the results meet three conditions required for the optimal collocation.

Table 4 Estimated minimum distance between satellites

Satellites	Minimum distance, km
0–1	13.58
0–2	13.93
1–2	11.98

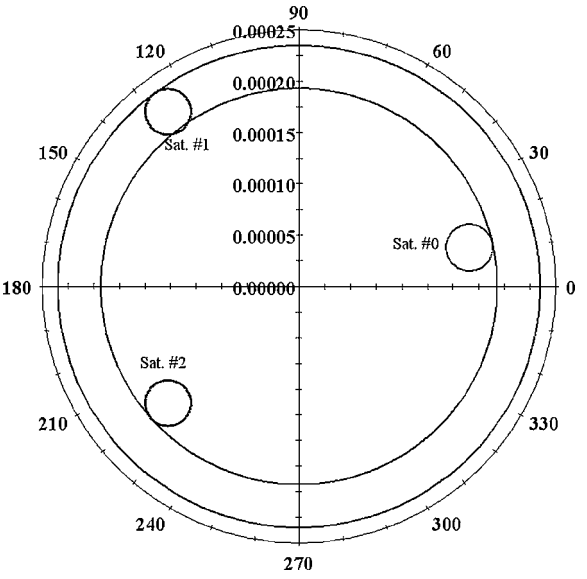

Fig. 4 Resulting positions of eccentricity circles.

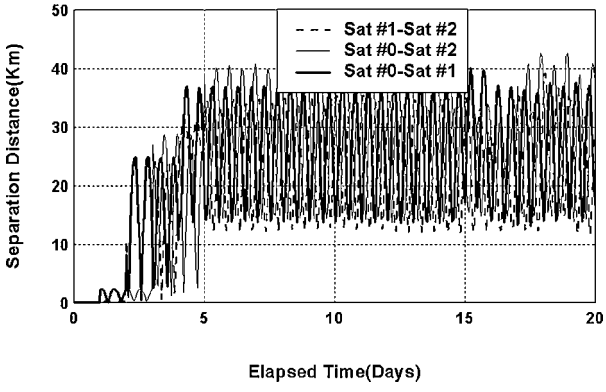

Fig. 5 Time history of the separation distances.

Table 4 shows the theoretically estimated values for the distances between satellites, whereas Fig. 5 displays the resultant distances between satellites from numerical simulation. The minimum distance of the simulation results in well coincident with the maximum radial separation distance of Table 4. The distance between two satellites is assumed zero at the initial time, and all satellites are placed with the same orbital elements. As the collocation procedure proceeds, the separation distances gradually converge to theoretically estimated values.

Conclusions

This Note presented a new station collocation parameter design technique based on a virtual dynamic model. The new methodology is applicable to collision-free operation of multiple geostationary satellites collocated at the same longitudinal slot. A minimum set of parameters was used as input, which automatically produces the optimal position of the eccentricity control circles by using the virtual dynamics. Simulation results illustrate that the proposed strategy properly calculates the positions of the eccentricity control circle for any number of satellites with guaranteed maximum separation distance. The advantage of the proposed technique is that the collocation of any number of satellites can be treated with natural extension of the current methodology.

Acknowledgment

The present work was supported by the National Research Laboratory Program (M1-0203-00-0006) of the Ministry of Science and Technology, Republic of Korea. The authors fully appreciate the financial support.

References

[1]Brüege, U., and Görlach, T., "Solution for the Geostationary Collocation Problem," AIAA Paper 93-3789, 1993.

[2]Carlini, S., and Graziani, F., "An Eccentricity Control Strategy for Coordinate Station Keeping," *Proceeding of the 3rd International Symposium on Spacecraft Flight Dynamics*, SP-326, edited by J. J. Hunt, ESA, Darmstadt, Germany, 1991, pp. 17–21.

[3]Maisonbe, L., and Dejoice, C., "Analysis of Separation Strategy for Colocated Satellite," *Proceeding of the 3rd International Symposium on Spacecraft Flight Dynamics*, SP-326, edited by J. J. Hunt, ESA, Darmstadt, Germany, 1991, pp. 5–9.

[4]Lee, B. S., Lee, J. S., and Choi, K. H., "Analysis of a Stationkeeping Maneuver Strategy for Collocation of Three Geostationary Satellites," *Control Engineering Practice*, Vol. 7, July 1999, pp. 1153–1161.

[5]Lee, B. S., and Choi, K. H., "Collocation of Two GEO Satellites and One Inclined GSO Satellite," *Aerospace Science Technology*, Vol. 4, April 2000, pp. 507–515.

[6]Eckstein, M. C., "On the Separation of Collocated Geostationary Satellites," German Space Operations Center, TN87-20, Wessling, Germany, Dec. 1987.

[7]Pocha, J. J., "Stationkeeping," *An Introduction to Mission Design for Geostationary Satellites*, 1st ed., D. Reidel, Dordrecht, The Netherlands, 1987, pp. 80–129.

C. McLaughlin
Associate Editor

Dual-Code Thin-Layer Parabolized Navier–Stokes Strategy for Supersonic Flows over Spinning Bodies

Omid Abouali,* Mohammad M. Alishahi,† and Homayoon Emdad‡
Shiraz University, 71344 Shiraz, Iran
and
Goodarz Ahmadi§
Clarkson University, Potsdam, New York 13699-5725

Nomenclature

E, F, G	=	inviscid fluxes
E_v, F_v, G_v	=	viscous fluxes
$\tilde{E}, \tilde{F}, \tilde{G}$	=	fluxes in general curvilinear coordinates
J	=	Jacobian of transformation
P	=	pressure
Q	=	primitive variable matrix
q_x, q_y, q_z	=	heat-conduction terms
u, v, w	=	velocities
V	=	volume
x, y, z	=	Cartesian coordinates
α	=	angle of attack
ξ, η, ζ	=	general curvilinear coordinates
τ_{ij}	=	tensor of stresses
ρ	=	specific mass

Received 26 June 2002; revision received 3 May 2003; accepted for publication 13 May 2003.

*Assistant Professor, Department of Mechanical Engineering.
†Professor, Department of Mechanical Engineering.
‡Assistant Professor, Department of Mechanical Engineering. Member AIAA.
§Professor, Department of Mechanical and Aeronautical Engineering.

Introduction

THIS study is concerned with developing a supersonic combined computer code to be used on microcomputers as an aerodynamic design tool in preliminary and middesign stages. The CPU time needed for solving the Navier–Stokes equations for compressible flows is very high and normally requires a large computer memory; thus, in most cases supercomputers are used for such extensive computational efforts.[1,2]

In preliminary design stages, however, extensive computer resources might not be available and/or might be too costly. In practice, some approximate forms of the Navier–Stokes equations are solved.[3] The thin-layer Navier–Stokes (TLNS) equations are derived by neglecting the viscous terms in a streamwise direction. Although the use of TLNS decreases the required computer time and memory, the required resources are still large. The parabolized Navier–Stokes (PNS) equations are obtained by further neglecting the unsteady terms in the TLNS equations. For supersonic flows the PNS equations have a hyperbolic–parabolic nature and can be solved using space-marching algorithms. Therefore, the solution proceeds plane by plane, considerably decreasing the required computer resources. Using the PNS equations, however, is limited to the cases of supersonic flows with small streamwise pressure gradients and a starting plane of data is required in all cases to initiate the computation. Also, certain modeling must be taken for the subsonic streamwise pressure gradient within the boundary layer to suppress the upstream propagation of information. Hence the PNS equations are not appropriate for blunt-body and wing-body problems because of the subsonic flow restriction.

One alternative is to use a dual-code combination, that is, using the PNS code in most of the region and the use of the TLNS code wherever the PNS is not applicable. Wood and Thompson[4] implemented such a combined solution procedure for hypersonic flow fields about blunted slender bodies using a TLNS code (LAURA[5]) in the nose region and a PNS code (UPS[6–8]) in the afterbody region. The application of integrated LAURA-UPS procedure was demonstrated for two slender blunted cones.

Sturek et al.[9] reported the application of a three-dimensional TLNS solver, which was a central-differencing technique to predict the Magnus force and moments for hemispherical and flattened blunt-nose configuration and the PNS code to compute the flow over the remainder of the spinning shell. Emdad et al.[10] developed a PNS code to provide solutions on supersonic spinning slender bodies at high Reynolds numbers and moderate angles of attack. This code is a finite volume, shock-capturing, upwind scheme with the Roe method[11] that is fully implicit and second-order accurate in the crossflow planes. An option was included for turbulence using the Baldwin–Lomax model[12] and its modifications. This code is used as a part of a dual-code strategy in this study.

Alishahi et al.[13,14] developed a TLNS code. Roe's method is used to discretize the inviscid terms[15,16] and central differencing for the viscous terms. Time-derivative terms are discretized with the explicit technique. The Baldwin–Lomax model[12] and Degani–Schiff modifications are used for turbulence modeling. The algorithm is based on a finite volume approach. This code is used as the other part of the dual code.

In this study a PNS code is combined with a TLNS code to solve supersonic flows around the spinning bodies. An interpolation subprogram receives the data from the TLNS code and then prepares the needed initial data plane for PNS code. The cases of a supersonic flow over a nonspinning and spinning secant-ogive at Mach number 3 are studied. The dual-code simulation results are compared with experimental data, and the results are in good agreement with experimental data. It is found that the dual-code computer time is one order of magnitude less than that of TLNS code at comparable accuracy and thus provides a useful tool in preliminary design stages. Application of this dual-code procedure to a wing-body combination